teases offer a potentially better target for therapeutic intervention than the prenyl-transferases. Like the prenyl-transferases, blocking of Rce1p function reduces but does not eliminate Ras function. Moreover, null mutations in either *RCE1* or *AFC1* or in both genes cause no obvious growth or viability defects, whereas mutations in prenyl-transferases cause cells to be either growth defective or dead, depending on the mutation. Thus, if these results in yeast translate to human cells, inhibitors of CAAX proteases may be more valuable therapeutic agents than inhibitors of prenyl-transferases.

REFERENCES AND NOTES

1. W. R. Schafer and J. Rine, *Annu. Rev. Genet.* **26**, 209 (1992); S. Clarke, *Annu. Rev. Biochem.* **61**, 355 (1992).
2. F. R. Khosravi *et al.*, *Proc. Natl. Acad. Sci. U.S.A.* **88**, 6264 (1991); B. T. Kinsella and W. A. Maltese, *J. Biol. Chem.* **267**, 3940 (1992); M. C. Seabra, J. L. Goldstein, T. C. Sudhof, M. S. Brown, *ibid.*, p. 14497.
3. A. A. Finegold *et al.*, *Proc. Natl. Acad. Sci. U.S.A.* **88**, 4448 (1991); B. T. Kinsella, R. A. Erdman, W. A. Maltese, *ibid.*, p. 8934.
4. P. J. Casey, *Curr. Opin. Cell. Biol.* **6**, 219 (1994); J. E. Rothman and F. T. Wieland, *Science* **272**, 227 (1996).
5. J. F. Hancock, K. Cadwallader, C. J. Marshall, *EMBO J.* **10**, 641 (1991); K. Kato *et al.*, *Proc. Natl. Acad. Sci. U.S.A.* **89**, 6403 (1992); A. D. Cox, M. M. Hisaka, J. E. Buss, C. J. Der, *Mol. Cell. Biol.* **12**, 2606 (1992).
6. F. Tamanoi, *Trends Biochem. Sci.* **18**, 349 (1993); N. E. Kohl *et al.*, *J. Cell Biochem. Suppl.* **22**, 145 (1995).
7. W. R. Schafer *et al.*, *Science* **249**, 1133 (1990).
8. L. Gutierrez, A. I. Magee, C. J. Marshall, J. F. Hancock, *EMBO J.* **8**, 1093 (1989); R. S. Marr, L. C. Blair, J. Thorner, *J. Biol. Chem.* **265**, 20057 (1990); A. Fujiyama and F. Tamanoi, *ibid.*, p. 3362; S. D. Perez, B. A. Gilbert, E. W. Tan, R. R. Rando, *Biochem. J.* **284**, 835 (1992); R. C. Stephenson and S. Clarke, *J. Biol. Chem.* **267**, 13314 (1992).
9. M. N. Ashby, D. S. King, J. Rine, *Proc. Natl. Acad. Sci. U.S.A.* **89**, 4613 (1992); Y. T. Ma and R. R. Rando, *ibid.*, p. 6275; C. A. Hrycyna and S. Clarke, *J. Biol. Chem.* **267**, 10457 (1992); G. F. Jang, K. Yokoyama, M. H. Gelb, *Biochemistry* **32**, 9500 (1993).
10. A. Fujiyama, K. Matsumoto, F. Tamanoi, *EMBO J.* **6**, 223 (1987); C. A. Hrycyna, S. K. Sapperstein, S. Clarke, S. Michaelis, *ibid.* **10**, 1699 (1991).
11. A. Bender and G. F. Sprague, *Cell* **47**, 929 (1986).
12. A parent strain for the autocrine selection JRY5312 (*MAT***a** *HML***a** *HMR***a** *sst2*Δ *ade2-1 lys2 leu2-3, 112 ura3-1 STE3*::*GAL1-STE3*::*HIS3 mfa1*Δ::hisG *mfa2*Δ::hisG) was derived from W303-1a (JRY2334). For the halo and protease assays and heat shock and localization experiments, we used the following W303-1a derivatives: JRY5314 (*MAT***a** *his3 leu2-3,112 trp1 ura3-1*), JRY5315 (JRY5314 *afc1*Δ::*HIS3*), JRY5316 (JRY5314 *rce1*Δ::*TRP1*), JRY5317 (JRY5314 *afc1*Δ::*HIS3 rce1*Δ::*TRP1*). The temperature sensitivity experiments were performed in W303 derivatives: JRY5318 (*MAT***a**, *ade2-1 leu2-3,112 trp1, ura3-1 ras1*Δ::*HIS3 ras2-23*^{ts}), JRY5319 (JRY5318 *afc1*Δ::*HIS3*), JRY5320 (JRY5318 *rce1*Δ::*TRP1*), and JRY5321 (JRY5318 *afc1*Δ::*HIS3 rce1*Δ::*TRP1*). All strains were generated by standard genetic and molecular methods (*16*).
13. The plasmid carrying the wild-type (CVIA) (pJR1555) form of **a**-factor was created by insertion of the Xba I–Sal I fragment of the *MFA1* gene into pRS416 [R. S. Sikorsky and P. Hieter, *Genetics* **122**, 19 (1989)] *URA3 CEN* plasmid. The CAMQ variant (pJR1556) of *MFA1* was created by site-directed mutagenesis with the synthetic oligonucleotide 5′-GGGACCCAG-CATGTGCTATGCAATAGTTTCTGCG-3′. Wild-type *RAS2* (pJR1039) and dominant *RAS2*^{val19} (pJR1040) genes were contained in the 1.9-kb Cla I–Hind III fragment inserted into pRS316 vector. The *GFP-RAS2* fusion plasmid was created by subcloning the Bam HI–Sal I fragment containing the open reading frame of *RAS2* fused in frame to *GFP* under control of the glyceraldehyde-3-phosphate dehydrogenase (*GPD*) promoter {pJW192 [J. L. Whistler, thesis, University of California at Berkeley (1996)]}, into Bam HI– and Sal I–cut YEplac195 vector [R. D. Gietz and A. Sugino, *Gene* **74**, 527 (1988)]. The Rce1p-GFP fusions were constructed by engineering Xba I restriction sites flanking the *RCE1* open reading frame by polymerase chain reaction (PCR) amplification with synthetic oligonucleotides (5′-ACGTA-AAAATCTAGAAAGGGTTAT-3′ and 5′-AACAG-CAATGTCTAGATTCTCAAC-3′). The PCR product was subcloned into an Xba I site of the constructs containing ~1-kb promoter fragments in front of the GFP open reading fame [*GAL1*- pACA51, *ERG12*-pACA5, and *MEV1*-pACA1 (Acacia Biosciences)].
14. L. J. Heilmeyer *et al.*, *Proc. Natl. Acad. Sci. U.S.A.* **89**, 9554 (1992).
15. E. C. Gaynor, H. S. Te, T. R. Graham, M. Aebi, S. D. Emr, *J. Cell Biol.* **127**, 653 (1994).
16. A null allele of *afc1* was constructed by replacing the 218–base pair (bp) Bgl II fragment of *AFC1* (GenBank accession Z49617) with a 1764-bp Bam HI fragment containing the yeast *HIS3* gene. A deletion of the entire *RCE1* gene (GenBank accession Z49260) was created by PCR amplification of the *TRP1* coding sequence with synthetic oligonucleotides (5′-CCTTTGATGATTTTATTACCTTTATTT-TAAGTTACTAAAATATCGAGATTGTACTGAGAG-TGCACC-3′ and 5′-AAACAGTTGTCATGGAGC-CTTCCTGTAATTGCTCATAAGCATGGTGTGCGG-TATTTCACACCGC-3′). The PCR product was used directly in one-step gene replacement to create *rce1*Δ::*TRP1* [R. Rothstein, *Methods Enzymol.* **194**, 281 (1991)].
17. All assays were performed as described [M. N. Ashby and J. Rine, *Methods Enzymol.* **250**, 235 (1995)]. In direct CAAX proteolysis assays, 2 μg of membrane extract was incubated in 50 μl of 80 mM tris-HCl (pH 7.4), 1 mM phenylmethylsulfonyl fluoride (PMSF) reaction buffer with 0.5 nmol of a synthetic peptide KWD-PA(S-*trans*-*trans*-farnesyl)CV[4,5-^{3}H]IA (47 mCi/mmol) (K, Lys; W, Trp; D, Asp; P, Pro; A, Ala) and 20 μg of bovine serum albumin (BSA) for 1 hour at 37°C. After heat inactivation the RACE activity was measured by scintillation counting of cleaved tripeptide eluted from C_{18} cartridges (Analtech). In coupled proteolysis-methylation assays, 50 μg of protein was incubated with 1 nmol of Dansyl-WDPA(S-*trans*-*trans*-farnesyl)CVIA substrate and 1 nmol of [^{14}C]SAM (M, Met) in 100 mM tris-HCl (pH 7.4), 1 mM PMSF reaction buffer for 1 hour at 37°C. After addition of 50 μl of 1 M NaOH–1% SDS, the amount of newly formed hydrolyzed methyl esters was measured by scintillation counting.
18. V. L. Boyartchuck, M. N. Ashby, J. Rine, data not shown.
19. T. Kataoka *et al.*, *Cell* **40**, 19 (1985).
20. D. Broek *et al.*, *ibid.* **41**, 763 (1985).
21. H. Mitsuzawa, I. Uno, T. Oshima, T. Ishikawa, *Genetics* **123**, 739 (1989).
22. J. E. Buss, P. A. Solski, J. P. Schaeffer, M. J. MacDonald, C. J. Der, *Science* **243**, 1600 (1989); W. R. Schafer *et al.*, *ibid.* **245**, 379 (1989).
23. J. Inglese, W. J. Koch, M. G. Caron, R. J. Lefkowitz, *Nature* **359**, 147 (1992); C. A. Parish and R. R. Rando, *Biochemistry* **35**, 8473 (1996).
24. C. W. Cody, D. C. Prasher, W. M. Westler, F. G. Prendergast, W. W. Ward, *Biochemistry* **32**, 1212 (1993).
25. B. He *et al.*, *Proc. Natl. Acad. Sci. U.S.A.* **88**, 11373 (1991); L. E. Goodman *et al.*, *ibid.* **87**, 9665 (1990).
26. M. N. Ashby, P. R. Errada, V. L. Boyartchuk, J. Rine, *Yeast* **9**, 907 (1993); S. Sapperstein, C. Berkower, S. Michaelis, *Mol. Cell. Biol.* **14**, 1438 (1994).
27. R. C. Stephenson and S. Clarke, *J. Biol. Chem.* **267**, 13314 (1992); J. A. Thissen and P. J. Casey, *ibid.* **268**, 13780 (1993).
28. K. Kuchler and J. Thorner, *Curr. Opin. Cell Biol.* **2**, 617 (1990).
29. N. E. Kohl *et al.*, *Nature Med.* **1**, 792 (1995).
30. G. F. Sprague Jr., *Methods Enzymol.* **194**, 77 (1991).

31. We thank G. Sprague Jr. for providing the GAL-STE3 construct, H. Mitsuzawa for the *ras2-23* strain, J. W. Whistler for the GFP-Ras2p fusion, P. K. Herman for strains, D. King for peptide synthesis, R. Schekman and J. Thorner for critical reading of the manuscript, and all members of the Rine laboratory for support. Supported in part by NIH grant GM35827 (J.R.), California Tobacco Related Disease Research Program fellowship 4FT-0083, Acacia Biosciences, Incorporated (M.N.A.), E. B. Babckock Scholarship, and H. and E. K. Davis Memorial Fellowship (V.L.B.).

23 September 1996; accepted 18 February 1997

Crystal Structure of Protein Farnesyltransferase at 2.25 Angstrom Resolution

Hee-Won Park, Sobha R. Boduluri, John F. Moomaw, Patrick J. Casey, Lorena S. Beese*

Protein farnesyltransferase (FTase) catalyzes the carboxyl-terminal lipidation of Ras and several other cellular signal transduction proteins. The essential nature of this modification for proper function of these proteins has led to the emergence of FTase as a target for the development of new anticancer therapy. Inhibition of this enzyme suppresses the transformed phenotype in cultured cells and causes tumor regression in animal models. The crystal structure of heterodimeric mammalian FTase was determined at 2.25 angstrom resolution. The structure shows a combination of two unusual domains: a crescent-shaped seven-helical hairpin domain and an α-α barrel domain. The active site is formed by two clefts that intersect at a bound zinc ion. One cleft contains a nine-residue peptide that may mimic the binding of the Ras substrate; the other cleft is lined with highly conserved aromatic residues appropriate for binding the farnesyl isoprenoid with required specificity.

Posttranslational modification by a 15-carbon farnesyl isoprenoid is essential for the activity of a number of proteins that are central in the functioning of eukaryotic cells. These include Ras guanosine triphosphatases (GTPases), nuclear lamins, and several proteins involved in visual signal transduction (*1*). Addition of the farnesyl

group is required for localization of these proteins to the cell membrane; for example, the farnesylation of oncogenic variants of Ras is required for transformation of cells to a tumorigenic state (*2–4*). Inhibitors of FTase, the enzyme that catalyzes the farnesylation reaction, are sought because of their potential as chemotherapeutic agents (*5*); for example, FTase inhibition results in tumor regression in mice (*6*). We have now solved the crystal structure of rat FTase, which shares 97% sequence identity with the human enzyme.

FTase is a heterodimer consisting of 48-kD (α) and 46-kD (β) subunits (*7*); the same α subunit is also a component of a related enzyme, protein geranylgeranyltransferase type I (GGTase-I), which adds a 20-carbon isoprenoid group (*8*). Both FTase and GGTase-I use an isoprenoid diphosphate [farnesyl diphosphate (FPP) or geranylgeranyl diphosphate (GGPP), respectively] to modify the substrate through a thioether linkage to an invariant cysteine residue fourth from the COOH-terminus in a sequence motif commonly referred to as the "CAAX box." In this motif the second and third residues are small aliphatic amino acids. The two zinc metalloenzymes are specific for the COOH-terminal residue. FTase recognizes proteins that contain Ser, Met, Ala, or Gln at this position, whereas GGTase-I prefers proteins that terminate in Leu (*1*, *9*). A direct involvement of the zinc ion in catalysis (*10*) is supported by results of several studies; the most compelling is the recent finding that the thiol group of a CAAX peptide substrate directly coordinates the metal atom in a ternary complex (*11*).

In the crystal structure of FTase that we describe here, a single zinc ion is located at a junction between a hydrophilic surface groove near the subunit interface and a deep cleft in the β subunit lined with aromatic residues. This hydrophobic cleft, together with the location of a bound noncognate peptide, has allowed us to deduce the probable location of the isoprenoid and natural peptide substrate binding sites.

Fully active FTase was produced in Sf9 cells and purified as described (*12*). The crystal structure of heterodimeric FTase was determined to a resolution of 2.25 Å by multiple isomorphous replacement (MIR) and anomalous scattering with three heavy-atom derivatives (*13*) (Table 1), solvent flattening (*14*), phase combination (*15*), and crystallographic refinement (*16*).

The secondary structure of both the α and β subunits is largely composed of α helices (Fig. 1). Helices 2 to 15 of the α subunit are folded into seven successive pairs that form a series of right-handed antiparallel coiled coils. These "helical hairpins" are arranged in a double-layered, right-handed superhelix resulting in a crescent shaped subunit that envelops part of the β subunit. This unusual structure has also been observed in bacterial muramidase (*17*) and lipovitellin-phosvitin (*18*). All the helices in one layer are approximately parallel to each other and antiparallel to the helices in the adjacent layer. Twelve α helices of the β subunit are folded into an α-α barrel (Fig. 2). The α-α barrel structure is also unusual and has been seen in glycoamylase, bacterial cellulase, and endoglucanase CelA (*19*). A core of six parallel helices (3β, 5β, 7β, 9β, 11β, and 13β) forms the inner portion of the barrel. Six additional helices (2β, 4β, 6β, 8β, 10β, and 12β) interconnect the inner core of helices and form the outside of the helical barrel. The peripheral six helices are parallel to each other and antiparallel to the six core helices. One end of the barrel is blocked by a loop formed by residues 399β to 402β. The opposite end is open to the solvent, forming a deep cleft in the center of the

Table 1. Summary of FTase structure determination. Complete diffraction data were measured at −177°C with an *R*-axis II image plate system mounted on a Rigaku RU-200 rotating anode generator. Data reduction, merging, and scaling were accomplished with the programs DENZO and SCALEPACK (*36*). Three heavy-atom derivatives [(thimerosal (THAL), Di-iodobis-ethylenediamine-diplatinum II nitrate (PIP), and ethyl mercury phosphate (EMP)] were used to determine the crystal structures by MIR. A difference-Patterson map of the THAL derivative was calculated with the fast Fourier transform of the CCP4 suite (*21*). Two heavy-atom sites were identified by means of the real-space search program RSSP (*37*). These data were used to calculate single isomorphous replacement (SIR) phases at 5 Å resolution with MLPHARE (*38*). Difference Fourier synthesis with the SIR phases revealed five additional sites for the THAL derivative, three sites for the PIP derivative, and five sites for the EMP derivative. The MIR phases calculated at 3 Å resolution with all the derivative data had an overall mean figure of merit of 0.41. The phasing power for the PIP derivative was 1.0 at 4.5 Å resolution. Because of the high solvent content of the crystal (68% solvent) these phases were substantially improved with DM (*14*), a solvent-flattening density modification procedure. An atomic model was built with the program O (*39*) and refined in X-PLOR (*16*). Phase combination by means of SIGMAA (*15*) further improved the maps during building and refinement. The FTase structure contains 315 residues from the α subunit (residues 55 to 369) and 415 residues from the β subunit (residues 23 to 437). Disordered in the crystal are 54 residues at the NH_2-terminus (proline-rich domain) and 8 residues at the COOH-terminus of the α subunit. Twenty-two residues at the NH_2-terminus of the β subunit are not traced, although some disconnected electron density is visible. A zinc ion was fit into the highest peak in a $|F_o| - |F_c|$ difference map (5σ) (where F_o is the observed and F_c the calculated structure factor) before addition of water molecules. The final model contains 350 water molecules with a B factor less than 60 Å^2.

Data collection	Native	THAL	PIP	EMP
Resolution (Å)	25.0–2.25	25.0–3.00	25.0–3.00	25.0–3.00
Reflections				
Total (*N*)	442,035	304,521	314,332	264,751
Unique (*N*)	72,321	31,319	30,903	31,115
R_{sym}* (%)	4.9	6.0	10.5	6.0
Completeness (last shell†)	98.1 (87.6)	100 (99.9)	99.7 (99.3)	100 (99.9)
Derivatives				
Concentration (mM)		2	0.5	2
Soaking time (hours)		2	6.7	2
$\langle \Delta F \rangle / \langle F \rangle$‡ (%)		13.4	22.8	36.6
Phasing power§		0.92	0.41	1.23

Refinement statistics		Stereochemistry	
Resolution (Å)	6.0–2.25	rmsd bond lengths (Å)	0.01
Completeness of reflections [$F > 1\sigma(F)$] (%)	85.1	rmsd bond angles (degrees)	1.74
Number of reflections [$F > 1\sigma(F)$]	62,497		
R_{work}‖ (%)	21.7	Residues from Ramachandran plot (%)	
R_{free}‖ (%)	26.9	Most favored regions	89.3
Number of atoms	6,291	Additional allowed regions	10.7
Average B factor (Å^2)	28.9	Disallowed regions	0.0

*$R_{sym} = \Sigma\Sigma_j |I_j| - \langle I \rangle | / \Sigma | \langle I \rangle |$, where I_j is the intensity measurement for the reflection j, and $\langle I \rangle$ is the mean intensity for multiply measured reflections. †The last shell is between 2.31 and 2.25 Å resolution in the native data and between 3.08 and 3.0 Å resolution in derivative data. ‡$\langle \Delta F \rangle / \langle F \rangle = \Sigma_{hkl}(| \langle F_{hkl,p} \rangle - \langle F_{hkl,ph} \rangle |) / \Sigma_{hkl} \langle F_{hkl,p} \rangle$, where $\langle F_{hkl,p} \rangle$ and $\langle F_{hkl,ph} \rangle$ are the mean structure factor amplitudes of the native and the derivative. §Phasing power = $\langle F_h \rangle / E$, where $\langle F_h \rangle$ is the root mean square (rms) heavy-atom structure factor and E is the residual lack of closure error. ‖$R_{work, free} = \Sigma ||F_o| - |F_c|| / \Sigma |F_o|$, where the crystallographic and free R factors are calculated from the working and free reflection sets. The free reflections (5% of the total) were held aside throughout refinement.

H.-W. Park, S. R. Boduluri, P. J. Casey, L. S. Beese, Department of Biochemistry, Duke University Medical Center, Durham, NC 27710, USA.
J. F. Moomaw and P. J. Casey, Department of Molecular Cancer Biology, Duke University Medical Center, Durham, NC 27710, USA.
*To whom correspondence should be addressed.

barrel. The enzymatic active sites of other α-α barrel proteins are located in such clefts.

Multiple sequence alignment analysis of mammalian and yeast α subunits revealed five tandem repeats (*20*). Each repeat consists of two highly conserved regions separated by a divergent region of fixed length. These repetitive sequence motifs appear in the first five helical hairpins. The second α helix of each helical pair contains an invariant Trp residue that, together with other hydrophobic residues, forms the hydrophobic core of the hairpin. The conserved sequence Pro-X-Asn-Tyr (*20*) (where X is any amino acid) is found in the turns connecting two helices of the coiled coil. These turns form part of the interface with the β subunit. Internal repeats of glycine-rich sequences also have been identified in the β subunits of other protein prenyltransferases (*20*). These repeats correspond to the loop regions that connect the COOH-termini of the peripheral helices with the NH_2-termini of the core helices in the barrel.

The heterodimer is stabilized by an extensive subunit interface that buries about 3300 $Å^2$ of solvent-accessible surface area (*21*). Many of the polar interactions between subunits involve highly conserved residues found in the internal sequence repeats. Although the size of the subunit in-

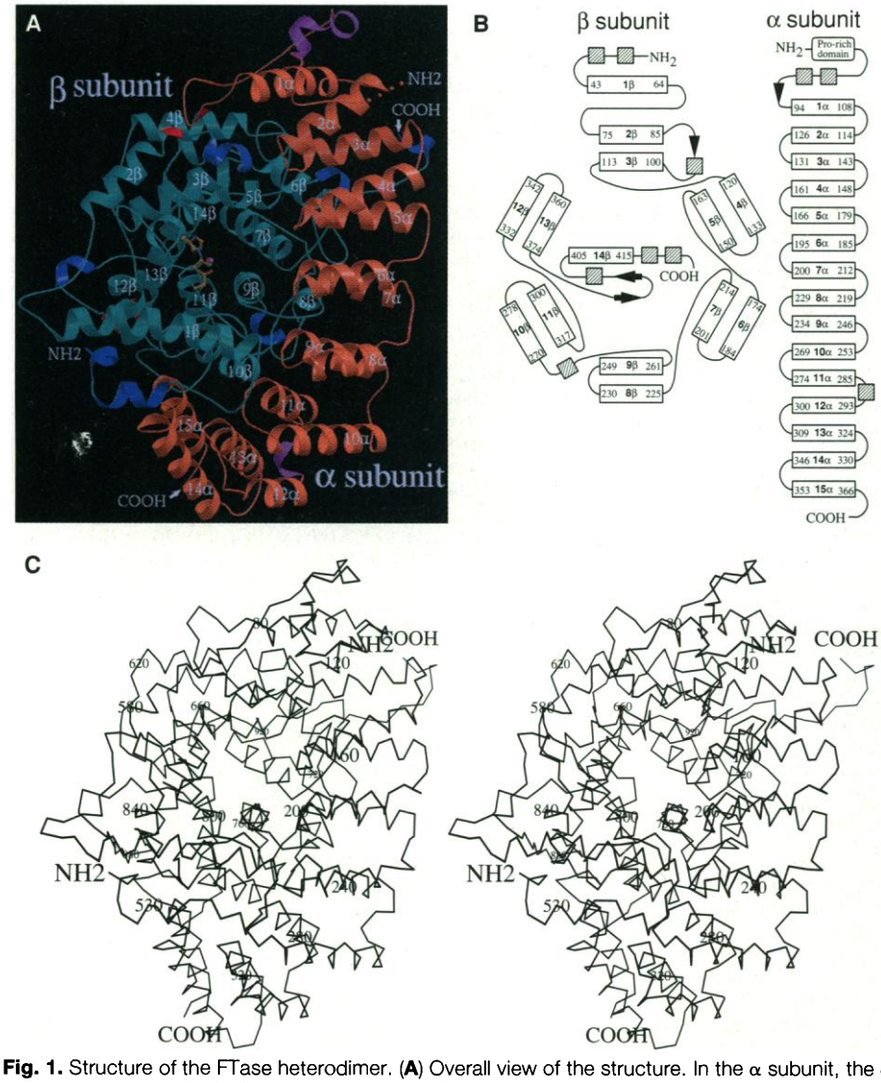

Fig. 1. Structure of the FTase heterodimer. (**A**) Overall view of the structure. In the α subunit, the α helices are orange, 3_{10} helices are magenta, and the β strand is red. In the β subunit, the α helices are cyan, 3_{10} helices are blue, and the β strands are red. The zinc ion is a magenta sphere and its three amino acid ligands are yellow. The secondary structures of the α subunit include 15 α helices, 3 short 3_{10} helices, and a short β strand. The β subunit contains 14 α helices, 7 short 3_{10} helices, and 3 short β strands [MOLSCRIPT (*40*) and RASTER3D (*41*)]. (**B**) Topology diagram. The open boxes represent α helices, the striped boxes 3_{10} helices, and the arrows β strands. In both subunits, the residue numbers for α helices are shown. Each of the 15 helices (1α to 15α) of the α subunit are 8 to 17 residues in length, and the connecting loops are 4 to 8 residues. Helices 1β to 14β of the β subunit contain between 9 and 22 residues. In the α subunit, the three 3_{10} helices are four to five residues in length (65α–69α, 70α–73α, and 288α–291α). A three-residue β strand (89α–91α) in the α subunit interacts with a β strand (87β–89β) in the β subunit at the subunit interface. In the β subunit, each of seven 3_{10} helices consists of less than seven residues (23β–27β, 28β–34β, 91β–96β, 264β–268β, 389β–393β, 423β–427β, and 433β–437β) and the three β strands are less than four residues in length (87β–89β, 375β–378β, and 381β–384β). The NH_2-terminal proline-rich domain (residues 1 to 54) is disordered in the crystal. The secondary structure elements were assigned with the program PROCHECK (*42*). (**C**) Cα stereo diagram.

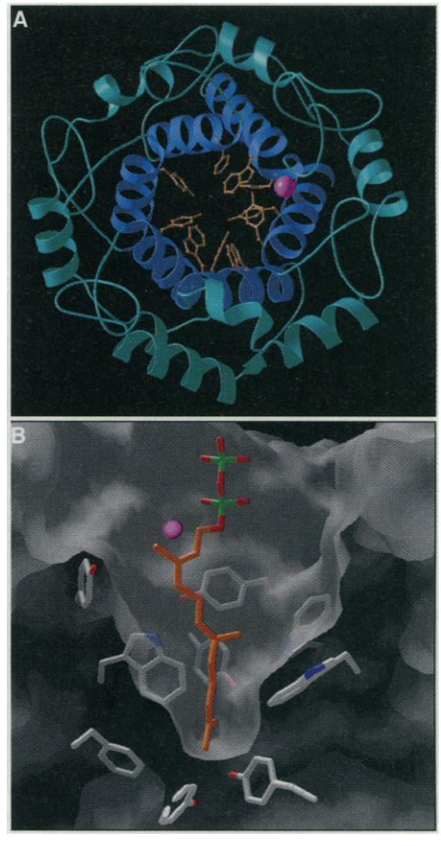

Fig. 2. The β subunit. (**A**) Aromatic pocket in the center of the α-α barrel of the β subunit. This view is a 90° clockwise rotation relative to Fig. 1A. Only helices 2β to 13β are shown. Yellow, the nine aromatic residues that line the pocket; magenta, the zinc ion [MOLSCRIPT (*40*) and RASTER3D (*41*)]. (**B**) A portion of the solvent-accessible surface showing some of the aromatic residues that line the putative FPP binding pocket. FPP is modeled with the isoprenoid in the hydrophobic cleft and the diphosphate moiety positioned near the zinc. The carbon atoms of FPP are yellow, oxygens are red, and phosphates are green. The program INSIGHT II (*43*) was used to construct an energy-minimized model of FPP and GRASP (*44*) was used to calculate the accessible surface.

terface is typical for an oligomeric protein, the number of hydrogen bonds is about double the normal number (*22*). In typical oligomeric proteins, subunit interfaces contain 65% nonpolar atoms (*22*). The FTase interface is unusual in that it is composed of 54% nonpolar residues, 29% polar atoms, and even 17% charged groups.

A single zinc ion binding to the β subunit is near the subunit interface. The zinc is coordinated by β subunit residues $Asp^{297\beta}$ and $Cys^{299\beta}$ located in the NH_2-terminal flanking loop region of helix 11β, $His^{362\beta}$ in helix 13β, and a water molecule. The $Asp^{297\beta}$ forms a bidentate ligand, resulting in a distorted pentacoordinate geometry. The zinc is bound at full occupancy with a B factor of 29.8 $Å^2$, comparable with the surrounding protein residues. The water molecule is well ordered and refined to a B factor of 17 $Å^2$. All three protein ligands are identical in the six known sequences of the β subunit (*23*). The mutation $Cys^{299\beta}$ to Ala affects zinc binding and abolishes catalytic activity (*24*). Because a near universal hallmark of catalytic zinc atoms is the presence of an open coordination sphere that includes a water molecule, in contrast to structural zinc atoms, which are coordinated by protein ligands alone (*25*), we conclude that the zinc binding site observed in the crystal marks the location of the active site.

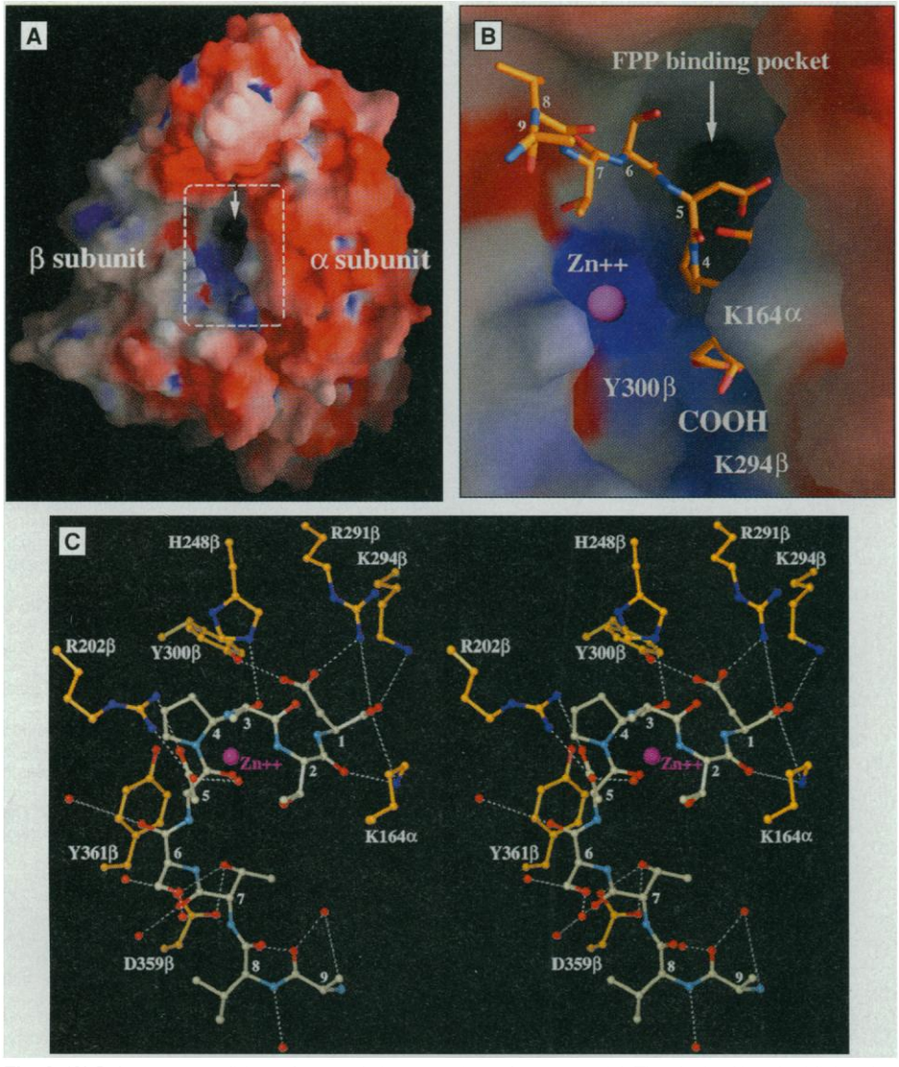

Fig. 3. (**A**) Solvent-accessible surface and electrostatic surface potential. The dashed box highlights the cleft where the nonapeptide binds. The most negative electrostatic surface potential (−10 kT) is colored red. The most positive electrostatic surface potential (10 kT) is blue. The orientation is similar to that of Fig. 1. The arrow indicates the putative FPP binding site [GRASP (*44*)]. (**B**) Close-up view of the nonapeptide binding cleft bounded by the dashed lines in (A). The COOH-terminus and six residues of the nonapeptide (Ala^9-Val^8-Thr^7-Ser^6-Asp^5-Pro^4) are visible. Atom colors for the nonapeptide are coral, carbons; red, oxygen; light blue, nitrogen; and zinc, magenta. (**C**) Stereo view of the nonapeptide (COOH-terminus of a symmetry-related β subunit). The nonapeptide is numbered from the COOH-terminus. Atom colors in the nonapeptide are coral, carbons; orange, oxygen; and light blue, nitrogen. Atom colors of residues forming the binding pocket are khaki, carbons; red, oxygen; and blue, nitrogen. Zinc is a magenta sphere. Water molecules are red spheres. Dotted lines represent potential hydrogen bonds.

Cross-linking studies indicate that the binding sites for both protein and isoprenoid substrates reside on the β subunit (*26*, *27*). The location of the binding sites for the two substrates, the COOH-terminal CAAX peptide and FPP, can be inferred from the presence of two clefts that differ in their surface properties and that intersect at the active site marked by the bound zinc ion. One cleft runs parallel to the rim of the α-α barrel near the subunit interface. It is formed by a turn connecting helices 4α-5α in the α subunit and the loops connecting helices 8β-9β, 10β-11β, and 12β-13β in the β subunit. It is hydrophilic in nature, being lined with positively charged residues. The other cleft is nearly orthogonal to this peptide binding site and is formed by the central cavity of the α-α barrel. This pocket is hydrophobic in character, and for reasons discussed below, we consider it the site of FPP binding.

The hydrophobic cleft at the center of the α-α barrel is lined with 10 highly conserved aromatic residues: Trp (102β, 106β, 303β), Phe (253β, 302β), and Tyr (105β, 154β, 205β, 361β, 365β) (Fig. 2). Its inner diameter is 15 to 16 Å with a depth of 14 Å (*28*). At the top of this cleft, directly opposite the zinc ion, $Arg^{202\beta}$ in helix 7β is positioned such that it might interact with the phosphate moiety of the substrate. The length of FPP is such that if the terminal carbon of the isoprenoid binds at the bottom of the pocket, the diphosphate moiety could interact with the zinc atom (Fig. 2B).

This proposed binding site is consistent with several biochemical studies that suggest FPP binds exclusively to the β subunit (*23*, *26*). The marked change in fluorescence that accompanies the formation of the binary FTase-FPP complex (*29*) may be accounted for by the presence of three Trp residues in this cleft. A similar hydrophobic pocket formed with positively charged residues at the surface is observed in the proposed FPP binding site in FPP synthase (*30*).

The COOH-terminal nine residues (Ala^9-Val^8-Thr^7-Ser^6-Asp^5-Pro^4-Ala^3-Thr^2-Asp1-COOH) of a second β subunit, not part of the dimer but adjacent in the crystal lattice, was found to bind in the positively charged pocket of the β subunit (Fig. 3). This unusual arrangement was apparent even in the initial MIR electron density map, although the residues were not included in the model until the end of the refine-

ment. Although not common, such intersubunit peptide crossover has been observed previously in crystal structures such as that of factor Xa (*31*).

We propose that this nonapeptide mimics some aspects of normal CAAX peptide binding. Several lines of evidence support this proposal. The first four residues of this nonapeptide form a type I β turn (*32*), similar to the conformation for the natural CAAX peptides bound to FTase (*33*). The COOH-terminus of the nonapeptide is stabilized by side chains from both the α and β subunits, forming hydrogen bonds to $Lys^{164\alpha}$, $Arg^{291\beta}$, and $Lys^{294\beta}$. The hydrogen bond between the COOH-terminus and $Lys^{164\alpha}$ is consistent with the finding that the mutation of this residue abolishes FTase activity (*34*). In addition, there is experimental evidence that indicates the peptide binding site is located near the interface of the α and β subunits (*27*). The carboxylate group of Asp^{1} forms hydrogen bonds to $Arg^{291\beta}$ and $Tyr^{300\beta}$. The peptide conformation is stabilized by hydrogen bonds from its carbonyl oxygens and amide nitrogens, either to specific side chains ($Tyr^{300\beta}$, $His^{248\beta}$, $Tyr^{361\beta}$) or to water. In addition, peptide side chains of Asp^{5} and Thr^{7} form direct interactions with residues in the binding pocket (Fig. 3C).

The fourth residue in the nonapeptide (counted inward from the COOH-terminus) corresponds to the position of the cysteine to be farnesylated in a CAAX protein and is exactly in register with the zinc ion, adjacent to the presumed position of the FPP α phosphate. The thiol of a cysteine modeled onto the peptide backbone at this position can coordinate to the observed zinc ion. Although tempting, it is not possible to predict the mechanism of protein substrate specificity because the bound sequence differs significantly from any of the tetrapeptides found in the CAAX motif. Furthermore, binding of FPP, which is absent in this crystal, precedes peptide binding (*29*). Its presence may therefore also affect peptide conformation.

The affinity of a protein substrate for FTase is enhanced by the presence of multiple basic residues just upstream of the CAAX motif (the so-called polybasic region). For example, K-Ras has a much lower Michaelis constant than H-Ras, which lacks such a polybasic region (*35*). We observed a highly negatively charged region on the surface of FTase adjacent to the peptide binding site that is consistent with this observation (Fig. 3B).

FTase and GGTase-I share a common α subunit and carry out similar reactions with related prenyl substrates, usually with high specificity and little cross-reactivity. The crystal structure of FTase suggests how prenyltransferases discriminate between the related substrates FPP and GGPP. The farnesyl isoprenoid is 15 carbons in length, and the geranylgeranyl isoprenoid is 20 carbons. The distance between the bottom of the cleft and the zinc ion provides a molecular ruler that discriminates between the 15-carbon farnesyl group and the 20-carbon geranylgeranyl group. The depth of the putative isoprenoid binding pocket can accommodate the 15-carbon FPP, but it is too shallow for a 20-carbon GGPP. Whereas the isoprenoid of GGPP could also bind in the aromatic pocket, the additional five carbons of the geranylgeranyl moiety would place the pyrophosphate group out of register with the active site, preventing it from interacting properly during catalysis. This hypothesis is consistent with the finding that, although FPP and GGPP bind to FTase competitively, the geranylgeranyl isoprenoid is not transferred efficiently to the protein substrate (*10*).

REFERENCES AND NOTES.

1. F. L. Zhang and P. J. Casey, *Annu. Rev. Biochem.* **65**, 241 (1996); W. R. Schafer and J. Rine, *Annu. Rev. Genetics* **25**, 209 (1992); J. A. Glomset and C. C. Farnsworth, *Annu. Rev. Cell. Biol.* **10**, 181 (1994).
2. W. R. Schafer *et al.*, *Science* **245**, 379 (1989).
3. P. J. Casey, P. A. Solski, C. J. Der, J. E. Buss, *Proc. Natl. Acad. Sci. U.S.A.* **86**, 8323 (1989).
4. J. F. Hancock, A. I. Magee, J. E. Childs, C. J. Marshall, *Cell* **57**, 1167 (1989).
5. G. L. James *et al.*, *Science* **260**, 1937 (1993); N. E. Kohl *et al.*, *ibid.*, p. 1934; J. B. Gibbs, A. Oliff, N. E. Kohl, *Cell* **77**, 175 (1994); J. E. Buss and J. C. Marsters, *Chem. Biol.* **2**, 787 (1995).
6. N. E. Kohl *et al.*, *Nature Med.* **1**, 792 (1995).
7. Y. Reiss, J. L. Goldstein, M. C. Seabra, P. J. Casey, M. S. Brown, *Cell* **62**, 81 (1990); W.-J. Chen, D. A. Andres, J. L. Goldstein, D. W. Russell, M. S. Brown, *ibid.* **66**, 327 (1991); W.-J. Chen, D. A. Andres, J. L. Goldstein, M. S. Brown, *Proc. Natl. Acad. Sci. U.S.A.* **88**, 11368 (1991).
8. M. C. Seabra, Y. Reiss, P. J. Casey, M. S. Brown, J. L. Goldstein, *Cell* **65**, 429 (1991); F. L. Zhang *et al.*, *J. Biol. Chem.* **269**, 3175 (1994).
9. S. L. Moores *et al.*, *J. Biol. Chem.* **266**, 14603 (1991).
10. Y. Reiss, M. S. Brown, J. L. Goldstein, *ibid.* **267**, 6403 (1992); F. L. Zhang, J. F. Moomaw, P. J. Casey, *ibid.* **269**, 23465 (1994); J. F. Moomaw and P. J. Casey, *ibid.* **267**, 17438 (1992); P. J. Casey and M. C. Seabra, *ibid.* **271**, 5289 (1996).
11. C.-C. Huang, P. J. Casey, C. A. Fierke, *ibid.* **272**, 20 (1997).
12. W.-J. Chen, J. F. Moomaw, L. Overton, T. A. Kost, P. J. Casey, *ibid.* **268**, 9675 (1993).
13. Rat FTase was purified from an Sf9 expression system scaled up to 16 liters (*13*). FTase crystals were grown at 17°C from hanging drops containing a mixture of protein solution [4 to 16 mg of FTase per milliliter in 20 mM KCl, 10 mM ZnCl, 10 mM dithiothreitol, 20 mM tris-HCl (pH 7.7)] and reservoir solution [13 to 15% (w/v) PEG-8000, 200 mM ammonium acetate (pH 7.0)] and equilibrated against the reservoir solution by vapor diffusion. The FTase crystals were hexagonal and belong to the space group $P6_5$ with unit cell dimensions $A = B = 167.06$ Å, and $C = 97.90$ Å. There is one FTase heterodimer in the asymmetric unit.
14. K. Cowtan, *Newsl. Protein Crystallogr.* **31**, 34 (1994).
15. R. J. Read, *Acta Crystallogr.* **A42**, 140 (1986).
16. A. T. Brunger, *X-PLOR version 3.1. A System for X-ray Crystallography and NMR* (Yale Univ. Press, New Haven, CT, 1992).
17. A. M. Thunnissen *et al.*, *Nature* **367**, 750 (1994).
18. R. Raag, K. Appelt, N. H. Xuong, L. Banaszak, *J. Mol. Biol.* **200**, 553 (1988).
19. P. M. Alzari, H. Souchon, R. Dominguez, *Structure* **4**, 265 (1996); A. Aleshin, A. Golubev, L. M. Firsov, R. B. Honzatko, *J. Biol. Chem.* **267**, 19291 (1992); A. E. Aleshin, C. Hoffman, L. M. Firsov, R. B. Honzatko, *J. Mol. Biol.* **238**, 575 (1994); M. Juy *et al.*, *Nature* **357**, 89 (1992).
20. M. Boguski, A. W. Murray, S. Powers, *New Biol.* **4**, 408 (1992).
21. Collaborative Computational Project No 4., *Acta. Crystallogr.* **D50**, 760 (1994).
22. J. Jainin, S. Miller, C. Chothia, *J. Mol. Biol.* **204**, 155 (1988).
23. C. A. Omer *et al.*, *Biochemistry* **32**, 5167 (1993).
24. H. W. Fu, J. F. Moomaw, C. R. Moomaw, P. J. Casey, *J. Biol. Chem.* **271**, 28541 (1996).
25. B. L. Vallee and D. S. Auld, *Biochemistry* **29**, 5647 (1990); D. W. Cristianson, *Adv. Protein Chem.* **42**, 281 (1991).
26. Y. Reiss *et al.*, *J. Biol. Chem.* **266**, 10672 (1991); Y. E. Bukhtiyarov, C. A. Omer, C. M. Allen, *ibid.* **270**, 19035 (1995); K. Yokoyama, P. McGeady, M. H. Gelb, *Biochemistry* **34**, 1344 (1995).
27. W. Ying, L. Sepp-Lorenzino, K. Cai, P. Aloise, P. S. Coleman, *J. Biol. Chem.* **269**, 470 (1994).
28. The distances were measured between the peptide backbones of opposite helices in the core.
29. E. S. Furfine, J. J. Leban, A. Landavazo, J. F. Moomaw, P. J. Casey, *Biochemistry* **34**, 6857 (1995).
30. L. C. Tarshis, M. Yan, C. D. Poulter, J. C. Sacchettini, *ibid.* **33**, 10871 (1994).
31. K. Padmenabhan *et al.*, *J. Mol. Biol.* **232**, 947 (1993).
32. The phi psi angles for an ideal type I β turn are −60°, −30°, −90°, and 0°. In the nonapeptide we observed these angles to be −44°, −24°, −83°, and 8°. The distortion from ideality may arise from the proline in the fourth position.
33. S. J. Stradely, J. Rizo, L. Gierasch, *Biochemistry* **32**, 12586 (1993).
34. D. A. Andres *et al.*, *J. Biol. Chem.* **268**, 1383 (1993).
35. G. L. James, J. L. Goldstein, M. S. Brown, *ibid.* **270**, 6221 (1995).
36. Z. Otwinowski, in *Proceedings of the CCP4 Study Weekend*, L. Sawyer, N. Isaac, S. Borley, Eds. (SERC Daresbury, Daresbury, UK, 1993), pp. 56–62.
37. S. Knight, thesis, Swedish University of Agricultural Sciences, Uppsala, 1989.
38. Z. Otwinowski, in *Isomorphous Replacement and Anomalous Scattering*, W. Wolf, P. R. Evans, A. G. W. Leslie, Eds. (Science and Engineering Research Council, Warrington, UK, 1991), p. 80.
39. T. A. Jones and M. Kjeldgaard, *O version 5.9. The Manual* (Uppsala University, Uppsala, Sweden, 1993).
40. P. J. Kraulis, *J. Appl. Crystallogr.* **24**, 946 (1991).
41. E. A. Merritt and M. E. P. Murphy, *Acta. Crystallogr.* **D50**, 869 (1994).
42. R. A. Laskowski, M. W. MacArthur, D. S. Moss, J. M. Thornton, *J. Appl. Crystallogr.* **26**, 283 (1993).
43. *INSIGHT II: User Guide* (Biosym Technologies, San Diego, CA, 1993).
44. A. Nicholls, *GRASP: Graphical Representation and Analysis of Surface Properties* (Columbia University, New York, 1992).

45. Supported by NIH grant GM52382, Searle Scholar Foundation, and Schering-Plough Research Institute to L.S.B., and by NIH grant GM46372 and Council for Tobacco Research grant 4064 to P.J.C. We thank G. Petsko for ethyl mercury phosphate, A. Mondragon for advice on freezing FTase crystals, J. Richardson for advice on structural homology, and H. W. Hellinga for discussions and editorial assistance. We also thank the Keck Foundation for support of the Levine Science Research Center at Duke University. The coordinates have been deposited with the Brookhaven Protein Data Bank.

6 November 1996; accepted 26 February 1997